Atmos. Meas. Tech. Discuss., doi:10.5194/amt-2016-181, 2016
Manuscript under review for journal Atmos. Meas. Tech.
Published: 12 August 2016

Atmospheric Measurement Techniques Discussions

Simultaneous retrieval of water vapour and temperature profiles and cirrus clouds properties from measurements of far infrared spectral radiance over the Antarctic Plateau

Gianluca Di Natale[1], Luca Palchetti[1], Giovanni Bianchini[1], and Massimo Del Guasta[1]

[1]Istituto Nazionale di Ottica - CNR

Correspondence to: Luca Palchetti (Luca.Palchetti@ino.it)

Abstract. The possibility to discriminate the contribution of the atmosphere and ice clouds by using spectral infrared measurements is a fundamental step to quantify the cloud effect in the climate models. The simultaneous retrieval of clouds and atmospheric parameters allows to take into account the possible correlations between the variables. In this paper we describe the development of a routine able to perform the simultaneous retrieval and its application to the analysis of the spectral measurements acquired by the REFIR-PAD (Radiation Explorer Far Infrared - Prototype for Applications and Development) spectroradiometer, operative from Antarctic Plateau since 2012. This routine is able to operate the retrieval with reduced computing time comparable with the REFIR-PAD data acquisition time. The analysis allowed to retrieve the water vapour and temperature profiles and the clouds optical and micro-physical properties, such as the generalised effective diameter (D_{ge}) and the ice water path (IWP), by exploiting the spectral band between 230−980 cm^{-1}. To simulate the radiative transfer, the LBLRTM (Line By Line Radiative Transfer Model) was integrated with a specific code based on the δ-Eddington two-stream approximation, and further the cirrus clouds single scattering properties were derived from a database for hexagonal column habits. In order to identify the ice clouds a back-scattering and depolarisation lidar was available on the site and allowed to infer the position and the cloud thickness used in the simulations. A climatology of the vertical profiles of water vapour and temperature, was performed by using the daily radiosounding available at the base and it was used to build the a priori and initial guess profiles used in the fitting routine. An optimal estimation method with a Levenberg-Marquardt approach was applied to perform the retrieval. The comparison of results with radiosoundings demonstrates that the retrieved atmospheric state is not disturbed by the clouds presence. Finally, the retrieved clouds parameters were compared with the statistical correlation between the cloud temperature (T_c) and the optical depth measured in Antarctica at Dumond D'Urville and the effective diameters with the ice water content (IWC) obtained in the Arctic region finding a general agreement.

1 Introduction

Cirrus clouds have a strong effect on the Earth Radiation Budget (Kiehl and Trenberth, 1997; Harries et al., 2008; Liou, 1986), however their radiative impact is still uncertain (Baran, 2007) since they show a very strong variability in the space extent as well as in the crystal size/shape distribution (Baran, 2009). As reported by Baran (2009), the Earth-atmosphere radiation balance, which manifests itself between surface warming and cooling, depends upon many different parameters characterising

Atmos. Meas. Tech. Discuss., doi:10.5194/amt-2016-181, 2016
Manuscript under review for journal Atmos. Meas. Tech.
Published: 12 August 2016

Atmospheric Measurement Techniques Discussions

cirrus clouds, such as geometrical thickness, particles size and shape distribution (PSD) of ice crystals and most of all the optical depth. Furthermore they cover permanently about 30% of the planet surface, reaching the 70% in tropical areas (Baran, 2007), so their climate effect is very important.

The characterisation of these clouds is still uncertain due to the very complex shapes of their particles and the difficulty to detect very small crystals (De Leon and Haigh., 2007). The strongest effect occurs in the atmospheric window ($8-12$ μm) region and it is highly dependent on the optical thickness, but the contribution of far infrared (FIR), below 667 cm^{-1} (>15 μm), is also important because in this region the spectrum is very sensitive to the variation of the effective diameter, in particular at small particle sizes ($\simeq 20-30$ μm of effective diameter). The sensitivity is increased in the FIR because the strong modulation of the imaginary part of the refractive index (Linch et al., 2002) of ice, which has a peak at 800 cm^{-1} and a minimum at 400 cm^{-1}.

This FIR portion is also very important since represents up to the 45% percent of the entire thermal flux emitted by the Earth (Harries et al., 2008). For this reason, its modulation by clouds has important effect on the energetic balance. However, below 667 cm^{-1} the effect of the cloud overlaps with the water vapour absorption band, hence it is difficult to disentangle the competing effects associated with them. Wide band spectral measurements are essential to try to separate the different component of the system.

In this paper we describe a retrieval procedure which uses the broad band spectrum between $230-980$ cm^{-1} to discriminate and evaluate simultaneously both the thermal contribution of the water vapour and cirrus clouds, and also the application to the analysis of the spectral measurements of the radiance emitted by the atmosphere, performed over the Antarctic Plateau in very dry conditions. REFIR-PAD (Radiation Explorer in Far InfraRed - Prototype for Applications and Development) spectroradiometer (Palchetti et al., 2005; Bianchini at al., 2006) is very suitable for this purpose since it is one of the few operative instruments able to detect the whole infrared atmospheric radiance between $100-1400$ cm^{-1} ($7-100$ μm), covering the entire pure rotational band of water vapour in the FIR. The instrument is installed at Dome-C, at the Italian-French station of Concordia, on the Antarctic Plateau (75°06′ S, 123°20′ E) at 3233 m a.s.l., and it is acquiring data of spectral radiance from the atmosphere almost continuously since December 2011, both in clear and cloudy sky conditions.

Simultaneous and ancillary measurements, performed by a back-scattering/depolarisation lidar (Del Guasta et al., 1993), daily radiosoundings and a weather station placed on the roof of the physics Shelter where REFIR-PAD is placed, were also used in the retrieval procedure. Since the Antarctica field campaign has been going on for more than three years by now, a very large database of spectral measurements about the Antarctic atmosphere (Palchetti et al., 2015) has been collected. The development of a retrieval algorithm able to analyse the entire database will allow to perform reliable statistics about the radiative contribution of the Antarctic atmosphere and ice clouds.

The modelling of the clouds is a hard problem to solve since the exact distributions of crystals size and habits are very unpredictable, that means clouds are very inhomogeneous in space and in the internal structure as well as in time. The strongest assumption, which is considered sufficiently reliable, is the approximation of a single uniform layer. The developed algorithm makes different assumptions to simplify and optimise the simulations. The δ-Eddington two-stream approximation was applied to simulate the radiative transfer through the cloud layer. The downwelling and upwelling radiance incident at the cloud top

Atmos. Meas. Tech. Discuss., doi:10.5194/amt-2016-181, 2016
Manuscript under review for journal Atmos. Meas. Tech.
Published: 12 August 2016

Atmospheric Measurement Techniques Discussions

and bottom respectively are simulated at each iteration by LBLRTM as well as the downward radiance propagating from the cloud to the observer. The retrieval code is an optimal estimation based on the Levenberg-Marquardt approach (Marquardt, 1963) in which the retrieved parameters are the effective diameters and ice water path (IWP) for the cloud and a few levels on the vertical profiles of water vapour and temperature. The a priori information is given by the seasonal climatology build through the daily radiosoundings and also takes into account the correlations between water vapour and temperature.

Section 2 introduces the modelling of the atmosphere in presence of ice clouds by using the single scattering properties derived from the database compiled by Fu (1996) for hexagonal column ice crystals. In Section 3, the procedure to retrieve the clouds properties and the atmospheric variables is illustrated, starting from the generation of the a priori climatological profiles and the variance-covariance matrix (VCM). Furthermore, the procedure to choice the atmospheric levels to be retrieved, is also explained as well. Finally, in Section 4, the retrieval performance is also discussed.

2 Modelling of the thermal radiance emitted by cirrus clouds

The modelling of the thermal spectral radiance emitted by the atmosphere in presence of cirrus clouds follows the work about the fitting cloud parameters by using the measurements carried out during Testa Grigia field campaigns in 2007 and 2011 (Palchetti et al., 2015).

The δ-Eddington two-stream approximation of the radiative transfer equation (RTE) for a thermally inhomogeneous scattering layer in case of zenith-looking configuration was used, as suggested by Deeter and Evans (1997):

$$\begin{aligned} I_E(0) = e^{-\tau} I(\tau) + \frac{D_b}{1-\beta}(1 - e^{\tau(\beta-1)}) \\ + \frac{D_+}{1-\lambda}(1 - e^{\tau(\lambda-1)}) \\ + \frac{D_-}{1+\lambda}(1 - e^{-\tau(\lambda+1)}) \end{aligned} \quad (1)$$

where $I_E(0)$ and $I(\tau)$ are the radiance at the cloud base and cloud top respectively. The coefficients D_-, D_+ and λ are reported in Appendix A of Deeter and Evans (1997) and they depend on the upwelling and downwelling radiance and the Planck functions B_0 and B_1 at the cloud top and bottom. They also depend on the single scattering properties such as the single scattering albedo ω, the asymmetry factor g and the optical depth (OPD) τ. The β coefficient is the slope of the exponential approximation as a function of τ (Fu, 1991; Fu and Liou, 1993) used for the form of the Planck function:

$$B_1 = B_0 e^{\beta\tau} \quad (2)$$

Different works have been performed to parametrise the single scattering properties for the large variety of ice crystal habits as a function of the micro-physics (Yang et al., 2001; Yang at al., 2005; Wiser and Yang, 1998). In this work an homogeneous distribution of crystal shapes represented by hexagonal columns was assumed and the approximation of single uniform layer for clouds was considered.

Atmos. Meas. Tech. Discuss., doi:10.5194/amt-2016-181, 2016
Manuscript under review for journal Atmos. Meas. Tech.
Published: 12 August 2016

Atmospheric Measurement Techniques Discussions

The single scattering coefficients depending on the micro-physical properties (D_{ge}, IWP) are given by Fu et al. (1998):

$$\begin{aligned} \tau &= \text{IWP}(a_0 + a_1/D_{ge} + a_2/D_{ge}^2), \\ \tau_a &= \frac{\text{IWP}}{D_{ge}}(b_0 + b_1 D_{ge} + b_2 D_{ge}^2 + b_3 D_{ge}^3), \\ g &= c_0 + c_1 D_{ge} + c_2 D_{ge}^2 + c_3 D_{ge}^3 \end{aligned} \tag{3}$$

where D_{ge} is the generalised effective diameter defined as (Fu, 1996):

$$D_{ge} = \frac{\int_{L_{min}}^{L_{max}} D^2 L n(L) dL}{\int_{L_{min}}^{L_{max}} (DL + \frac{\sqrt{3}}{4} D^2) n(L) dL} \tag{4}$$

D, L and $n(L)$ in Eq. (4) are the width, the maximum dimension and the size distribution of the ice crystals respectively. The coefficients a_i, b_j and c_k in Eq. (3) are tabulated in a specific database (Fu et al., 1998) between $3-100$ μm, and τ_a denotes the absorption optical depth. The single scattering albedo is obtained from the following relation:

$$\omega = 1 - \tau_a/\tau \tag{5}$$

The optical parameters are scaled according to (Baran, 2005):

$$\begin{aligned} \tau' &= (1 - \omega g^2)\tau \\ g' &= g/(1+g) \\ \omega' &= (1 - g^2)\omega/(1 - \omega g^2) \end{aligned} \tag{6}$$

and plotted in Fig. 1 as function of frequency for different values of D_{ge}.The figure shows that in the FIR the sensitivity of the scattering to the diameter variations for different effective diameters (15,30,60 and 100 μm) is higher than in the atmospheric window between $800-980$ cm^{-1}. The maximum of extinction occurs around at $700-800$ cm^{-1}, mainly due to the absorption effect.

Following ((Baran, 2007) and (Rathke and Fisher, 2000)), the final parameters to be used in the radiative transfer model described in the following sections, are further scaled to take into account the gas contribution in the cloud layer yielding:

$$\begin{aligned} \tau_t &= \tau + \tau_g \\ \omega'' &= \omega' \frac{\tau'}{\tau_t'} \\ g'' &= g' \frac{\tau'}{\tau_t'} \end{aligned} \tag{7}$$

where τ_g represents the extinction optical depth of the gases calculated by LBLRTM (Clough at al., 2005).

Atmos. Meas. Tech. Discuss., doi:10.5194/amt-2016-181, 2016
Manuscript under review for journal Atmos. Meas. Tech.
Published: 12 August 2016

Atmospheric Measurement Techniques Discussions

3 Retrieval algorithm

In the approximation of single uniform layer, the spectral contribution of cirrus clouds is completely determined by the vector of parameters (D_{ge}, IWP). The retrieved atmospheric variables are the values of the volume mixing ratio (VMR) of the water vapour and temperature at a few levels of the vertical profiles. The other levels of the profiles are linearly interpolated and the main unfitted molecular specie considered in the analysis is the carbon dioxide.

The atmosphere was modelled by using a grid of 52 levels with a very high resolution of 2,7,8,10,20 m in the very first layers above the instrument, reaching a very low resolution of 1 km in the upper part, close to the tropopause. The initial guesses of the water vapour and temperature as well as the a priori information are represented by the seasonal climatology performed in this work, and the carbon dioxide profile by the climatology performed by Remedios et al. (2007). The retrieval was limited in the spectral region between 230−980 cm^{-1} to include the pure rotational band of water vapour placed below 667 cm^{-1} and the vibro-rotational band of carbon dioxide taking into account the atmospheric window between 820−980 cm^{-1} and neglecting the ozone band above 1000 cm^{-1}.

In order to retrieve the atmospheric variables, we need to invert the equation:

$$\mathbf{y} = \mathbf{F}(\mathbf{x}) + \boldsymbol{\epsilon} \tag{8}$$

where $\mathbf{F}$ is the forward model, $\mathbf{y}$ and $\boldsymbol{\epsilon}$ are the vectors of the measurement and its uncertainty respectively and $\mathbf{x}$ is the state vector of the system composed of the atmosphere and the cloud. An optimal estimation approach is used for the retrieval of $\mathbf{x}$ by means of the minimisation of the cost function:

$$\chi^2 = (\mathbf{y} - \mathbf{F}(\mathbf{x}))^T \mathbf{S}_\epsilon^{-1} (\mathbf{y} - \mathbf{F}(\mathbf{x})) + (\mathbf{x} - \mathbf{x}_a)^T \mathbf{S}_a^{-1} (\mathbf{x} - \mathbf{x}_a) \tag{9}$$

where $\mathbf{x} = (D_{ge}, \mathrm{IWP}, \mathbf{U}, \mathbf{T})$ is the state vector with $\mathbf{U}$ and $\mathbf{T}$ vectors of selected levels on water vapour and temperature profiles and $\mathbf{x}_a$ the vector of the a priori information that we assumed coincident with the initial guess; $\mathbf{S}_\epsilon$ and $\mathbf{S}_a$ represent the VCM of the measurements and the a priori respectively calculated as follow (Ceccherini and Ridolfi, 2010):

$$(\mathbf{S}_\epsilon)_{ij} = \langle \boldsymbol{\epsilon}\boldsymbol{\epsilon}^T \rangle = \delta_{ij}(NESR_j^2 + (\sigma_F)_j^2) + \varepsilon_i \cdot \varepsilon_j \tag{10}$$

for the measurement, where the symbol $\langle \cdots \rangle$ denotes the expectation value, δ_{ij} is the identity matrix, NESR is the noise equivalent spectral radiance (Palchetti and Lastrucci, 2001), σ_F the error on the unfitted species and $\boldsymbol{\varepsilon}$ is the calibration error. On the right side of the equation, the term composed of NESR and σ_F denotes the statistical noise, whereas the term of products

Atmos. Meas. Tech. Discuss., doi:10.5194/amt-2016-181, 2016
Manuscript under review for journal Atmos. Meas. Tech.
Published: 12 August 2016

Atmospheric Measurement Techniques Discussions

$\epsilon_i \cdot \epsilon_j$ represents the systematic error given by the calibration uncertainty with correlation 1 as derived from the Planck law. On the other hand the VCM of a priori profiles was obtained as a block matrix:

$$\mathbf{S}_a = \begin{pmatrix} \mathbf{S}_{cld} & \mathbf{0} \\ \mathbf{0} & \mathbf{S}_{atm} \end{pmatrix} \tag{11}$$

where $\mathbf{S}_{cld}$ is the diagonal VCM for cloud parameters expressed as:

$$\mathbf{S}_{cld} = \begin{pmatrix} \sigma^2_{D_{ge}} & 0 \\ 0 & \sigma^2_{IWP} \end{pmatrix} \tag{12}$$

The $\mathbf{S}_{atm}$ matrix is the VCM of the atmosphere in which the off diagonal elements are not null and take into account the correlations between each atmospheric level and also between temperature and water vapour. We can note that the a priori correlation between atmosphere and cloud is set to be 0. The σ_F in Eq. (10) is obtained by means of the standard deviation σ_{CO_2} of the CO_2 profile (Remedios et al., 2007) and the derivative of the forward model with respect to the CO_2 volume mixing ratio. The standard deviations of D_{ge} and IWP in the 2x2 diagonal matrix in Eq. (12) were set to be large enough to not be serious constraints Turner (2005). If $\mathbf{x} = (\mathbf{U}, \mathbf{T})$ represents the vector of the atmospheric radiosounding of water vapour ($\mathbf{U}$) and temperature ($\mathbf{T}$) then the $\mathbf{S}_{atm}$ can be calculated from the expectation value:

$$(\mathbf{S}_{atm})_{ij} = \langle \boldsymbol{\sigma}_a \boldsymbol{\sigma}_a^T \rangle = \frac{1}{N-1} \sum_{k=1}^{N} [(x_{ik} - \bar{x}_i)(x_{jk} - \bar{x}_j)] \tag{13}$$

where $i, j = 1, \cdots, 104$, $\boldsymbol{\sigma}_a$ denotes the error of a priori and x_{ik} represents the value of the k-th water vapour profile at the i-th level if $i \leq 52$, or the k-th temperature profile at the $(i-52)$-th level if $52 < i \leq 104$. The $\bar{x}_i$ denotes the average at the i-th level of water vapour or $(i-52)$-th level of temperature calculated averaging a set of $N \simeq 90$ radiosoundings. From Eq. (13) derives that for the same index $i = j$ we find the corresponding variance.

The iterative formula (Marquardt, 1963; Palchetti et al., 2008; Bianchini at al., 2007), was implemented by using a Levenberg-Marquardt approach:

$$\begin{aligned} \mathbf{x}_{i+1} = \mathbf{x}_i + [\mathbf{K}_i^T \mathbf{S}_\epsilon^{-1} \mathbf{K}_i + \gamma \mathbf{D}_i + \mathbf{S}_a^{-1}]^{-1} \times \\ \{\mathbf{K}_i^T \mathbf{S}_\epsilon^{-1} (\mathbf{y} - \mathbf{F}(\mathbf{x}_i)) - \mathbf{S}_a^{-1} [\mathbf{x}_i - \mathbf{x}_a]\} \end{aligned} \tag{14}$$

where $\mathbf{x}_i$ is the vector state at the i-th iteration, γ is the regularization factor and $\mathbf{D}_i$ is the diagonal matrix (Gavin, 2015):

$$\mathbf{D}_i = \text{diag}(\mathbf{K}_i^T \mathbf{S}_\epsilon^{-1} \mathbf{K}_i) \tag{15}$$

Atmos. Meas. Tech. Discuss., doi:10.5194/amt-2016-181, 2016
Manuscript under review for journal Atmos. Meas. Tech.
Published: 12 August 2016

Atmospheric Measurement Techniques Discussions

and the matrix $\mathbf{K}_i$ is the Jacobian at the i-th iteration given by:

$$K_{ijl} = \frac{\partial F_j(\mathbf{x}_i)}{\partial x_l} \tag{16}$$

The form of matrix $\mathbf{K}_i$ at the i-th iteration is determined for i = 0 and in case of increasing χ^2 by means of the finite difference calculation and in case of decreasing χ^2 and in every $2n$ iterations (with n number of parameters) by using the Broyden rank1 update formula (Broyden, 1965) for the quasi-Newton methods:

$$\mathbf{K}_{i+1} = \mathbf{K}_i + [(\mathbf{F}(\mathbf{x}_{i+1}) - \mathbf{F}(\mathbf{x_i}) - \mathbf{K}_i\Delta\mathbf{x}_i)\Delta\mathbf{x}_i]/(\Delta\mathbf{x}_i^T \cdot \Delta\mathbf{x}_i) \tag{17}$$

with $\Delta\mathbf{x}_i = \mathbf{x}_{i+1} - \mathbf{x}_i$.

The VCM of the state vector $\mathbf{x}$ was provided by the the optimal estimation as follow (Rodgers, 2000):

$$\mathbf{S}_x = (\mathbf{K}^T\mathbf{S}_\epsilon^{-1}\mathbf{K} + \mathbf{S}_a^{-1})^{-1} \tag{18}$$

The upwelling and downwelling radiance incoming at the cloud bottom and top respectively were simulated at each iteration and they were used for the calculation of the coefficients λ, D_- and D_+ in Eq. (1) and, for the upwelling radiance coming from the ground, the emissivity of the surface was set to be 1 and the ground temperature was given by the Vaisala station placed on the roof of the physics Shelter.

3.1 Selected measurements and climatology

The measurements of the atmospheric radiance were performed by REFIR-PAD (Palchetti et al., 2015) with a time frequency of 12 minutes and a spectral resolution of 0.4 cm^{-1}. For the evaluation of the performance of the developed retrieval algorithm, a set of 15 spectra were selected in the year 2014 in coincidence as close as possible with the radiosounding performed at 12 UTC and in presence of ice clouds, identified by exploiting the logarithmic range corrected signal (RCS) and the depolarisation signal provided by the back-scattering lidar.

The lidar have 2 frequencies channels at 532 and 1064 nm respectively and allows to acquire data with a time resolution of 10 minutes, very close to the REFIR-PAD acquisition frequency. In Fig. 2 the colour maps of the RCS and depolarisation signals detected by the lidar for four selected days of the analysed spectra, one for each season, are shown. The red solid lines in the panels indicate when the acquisition of the spectrum was performed by REFIR-PAD. The first upper panel shows the passage of an ice cloud at 1.8 km of height with a geometrical thickness of about 1.4 km and the acquisition was made at 13:47 UTC on 12 February 2014. The ice cloud in the right upper panel occurred on 2 April 2014 at about 0.6 km of height with 1.4 km of thickness and the acquisition was performed at 11:36 UTC. The last two panels show the passage of ice clouds respectively on 10 August 2014 at 1 km with 2 km of thickness passed at 10:49 UTC and a cloud at 1.6 km with 0.7 km of thickness on 1 October 2014 at 11:59 UTC. The depolarisation signal ensures the presence of ice in the clouds as shown in

Atmos. Meas. Tech. Discuss., doi:10.5194/amt-2016-181, 2016
Manuscript under review for journal Atmos. Meas. Tech.
Published: 12 August 2016

Atmospheric Measurement Techniques Discussions

Fig. 3 and allows to exclude for example the cases of mixed-phase clouds, often occurring in the polar atmospheres (Turner, 2005; Turner et al., 2003).

The four climatological profiles of water vapour and temperature for the year 2014 are plotted in Fig. 4. In the right panel we can note the strong temperature inversion which occurs at around 500 m above the ground in Winter and Autumn and it is a peculiarity of the Antarctic atmosphere due to the very low temperatures, below -60 °C, reached at the ground level during these seasons. The water vapour VMR profiles also manifests a strong inversion in Winter and Autumn as shown in the left panel. The standard deviation σ of climatological profiles allowed to fix the limits of the retrieval domain and they were set to be 3-σ in order to take into account almost the totality of cases. Only for the ground level a larger limit was chosen since the variability of the very first layer, corresponding to the internal ambient of the physical shelter, and completely isolated from the external one. These limits represent the real physical domain in which the atmospheric variables can be varied by the retrieval routine.

3.2 Optimisation of the retrieved state vector

In order to determine how many degrees of freedom which better represent the atmospheric states and setting the retrieval levels, a study of the matrix $\widetilde{\mathbf{K}}$ given by:

$$\widetilde{\mathbf{K}} = \mathbf{S}_y^{-\frac{1}{2}} \mathbf{K} \mathbf{S}_a^{\frac{1}{2}} \tag{19}$$

was performed by means of the singular value decomposition:

$$\widetilde{\mathbf{K}} = \mathbf{U} \mathbf{\Sigma} \mathbf{V}^T \tag{20}$$

The analysis was performed by using the four seasonal climatological profiles, as shown in Fig. 4, composed of 52 levels interpolated on a grid with vertical resolution of 100 m to calculate the Jacobians with respect to the atmospheric variables in clear sky conditions.

The columns of $\mathbf{V}$ represent the eigenvectors of matrix $\widetilde{\mathbf{K}}\widetilde{\mathbf{K}}^T$ in the state space transformed by $\mathbf{S}_a^{-\frac{1}{2}}$ and to come back to the original state space we can transform the vectors by means of $\mathbf{S}_a^{\frac{1}{2}}$ (Rodgers, 2000), such that:

$$\mathbf{S}_a^{\frac{1}{2}} \widetilde{\mathbf{v}}_i = \mathbf{v}_i - \mathbf{x}_a \tag{21}$$

where $\widetilde{\mathbf{v}}_i$ are the columns of matrix $\mathbf{V}$. As shown by (Rodgers, 2000) the singular values of $\widetilde{\mathbf{K}}$ perfectly represent the signal to noise ratio and the number of singular values, which are greater than about unity represents the effective rank of the system. The singular values greater than unity correspond to the states which carry information about the parameters to be retrieved, indeed the lower ones don't bring information but only noise. The singular values also give the sensitivity to measure a singular vector Rodgers (2000). To avoid the oscillation in the retrieval, due to the strong variability in the lowest layers, only

Atmos. Meas. Tech. Discuss., doi:10.5194/amt-2016-181, 2016
Manuscript under review for journal Atmos. Meas. Tech.
Published: 12 August 2016

Atmospheric Measurement Techniques Discussions

the singular vectors which can be measured with a sensitivity greater than about 10% of the maximum value were took into account. These corresponds to the first two eigenvectors for water vapour and the first three for temperature for the all seasons as shown in Fig. 5. This means that only two levels of water vapour and three levels of temperature can be accurately retrieved.

The retrieval levels were set by selecting the back transformed eigenvectors which satisfy the above conditions and by studying where the overlap of maximums occurred. In Fig. 6 the back-transformed singular vector of $\widetilde{\mathbf{K}}$ for singular values greater than about unity of water vapour and temperature by using the winter climatology are shown. The retrieval levels above the ground are also reported in black-dashed line. The second level of temperature was set at about 10 meters above the ground to take into account the strong gradient in the very first layers. The grid levels of water vapour and temperature profiles were linearly interpolated between the fitted levels and the portion of the profile above the last level was simply scaled.

4 Results

Figure 7 shows the fitting results for the selected cases of Fig. 2. The measurements (black line) are compared with the synthetic spectra (red line) obtained by the fit, and the residuals are reported in the lower panels (green line). The first panel shows the atmospheric spectrum with an ice cloud composed of large particle sizes, the retrieval provided 47 μm of D_{ge}, and optical depth of 0.4. The following panels contain spectra with ice clouds with smaller diameters, precisely 34, 21 and 23 μm, and optical depths of 0.5, 1.1 and 0.6 respectively. The good fitting results, with a residual difference within the uncertainty of the measurement, shows that the simultaneous retrieval including the FIR portion of the spectrum allows to reduce the residual difference between model and measurement in comparison with techniques which use only the mid-infrared (MIR) Maestri et al. (2014). The comparison between the retrieved water vapour and temperature profiles with the radiosounding are reported in Fig. 8 for the same cases of Fig. 2. As we can see the retrieved profiles are generally in very good agreement with the radiosoundings. The differences in the first layers are mainly due to:

1. the strong variability occurring in the boundary layer.
2. the radiosonde launched not exactly close to the shelter, in which REFIR-PAD is placed.
3. the presence of a very strong gradient in the very first layers between the instrument, inside the shelter, and the external ambient.

The fitting results for the cirrus cloud optical and micro-physical properties are shown in Fig. 9 in which the time evolution of the clouds parameters is plotted. The retrieved effective particle diameters mostly variates between 20 and 50 μm, the temperature between -30 and -60 °C and the OPD between 0.05 and 1.1. The largest diameters occur in Summer when temperature is higher whereas the optical depths are generally lower than about 1, hence cirrus clouds are generally optically thin.

The retrieved cloud parameters were compared with two statistical correlations available for polar regions, where the cloud temperature is related to the optical depth and the ice water content to the effective diameter. The first relationship is represented

Atmos. Meas. Tech. Discuss., doi:10.5194/amt-2016-181, 2016
Manuscript under review for journal Atmos. Meas. Tech.
Published: 12 August 2016

Atmospheric Measurement Techniques Discussions

by an exponential function obtained from data acquired at Dumont D'Urville in 1993 (Del Guasta et al., 1993) for cirrus clouds with temperature lower than -30 °C, and is given by:

$$\tau = exp(a \cdot T_c + b) \tag{22}$$

with $a = 0.0284$ and $b = 0.2110$.

The second law correlates the effective diameter D_e with the ice water content (IWC) through a logarithmic relation given by (Liou, 2008):

$$D_e = exp(a + b \cdot ln(IWC) + c \cdot (ln(IWC))^2) \tag{23}$$

with a = 4.8510, b =0.33159 and c = 0.026189 are coefficients that are found for the Arctic region. The values of IWC are calculated from the retrieved IWP data reminding the assumption of single uniform layer as follow:

$$IWC = \frac{IWP}{\Delta z} \tag{24}$$

where Δz is the geometrical thickness of the cloud. The comparison between the retrieved parameters and statistical correlation laws shows a very good agreement, Fig. 10. The relationships of Eq. (22) and (23) were used to fit the retrieved data through the coefficient a, b, c, obtaining for the $T_c - \tau$ case, $a = 0.0200$ and $b = 0.0002$, and for the IWC $- D_e$ case, $a = 4.3114$,$b = 0.39111$, and $c = 0.052090$. The retrieval results again shows that the retrieved cloud parameters are in good agreement with the available statistics for polar regions.

5 Conclusions

In this work an efficient routine to operate the simultaneous retrieval of the atmospheric water vapour and temperature profiles and the cloud parameters, was developed and applied to the analysis of measurements performed over the Antarctic Plateau by using the spectral measurements in the far infrared carried out in 2014 by the REFIR-PAD Fourier spectroradiometer. The procedure exploited the whole spectral range between 230$-$980 cm^{-1} and allowed to retrieve simultaneously the atmospheric variables and the cloud optical and micro-physical properties such as the generalised effective diameters and the ice water path. The region below 667 cm^{-1} is very important because the modulation of the spectrum due to the clouds effect is very strong showing high sensitivity to the ice particles size.

The modelling of the atmosphere was performed by integrating the LBLRTM with a specific code based on the δ-Eddington two-stream approximation of the radiative transfer to take into account the effect of the clouds. A preliminary optimisation of the retrieved state vector was performed by means of the Jacobian matrix to set the best grid of levels on the water vapour and temperature profiles to be used in the retrieval procedure. A climatology was also performed by using daily radiosoundings available at the base to make a good a priori information.

Atmos. Meas. Tech. Discuss., doi:10.5194/amt-2016-181, 2016
Manuscript under review for journal Atmos. Meas. Tech.
Published: 12 August 2016

A good agreement was found between the atmospheric retrieved profiles of water vapour and temperature and the available simultaneous radiosoundings, and between retrieved cloud data and the statistical correlations available for polar regions. Clouds and ice detection was provided by the back-scattering/depolarisation lidar placed close to REFIR-PAD. A very good agreement of the residuals with the model was found and the retrieved cloud data were compared with the statistics performed at Dumont D'Urville correlating the optical depth to the temperature and the ice water content to the effective diameter.

This work has shown the capability to perform a simultaneous retrieval of the atmospheric state and the cloud parameters taking into account the possible correlations between the clouds and the atmosphere. The residual difference between models and measurements is within the measurement errors over the whole relevant spectral range of the emission including the FIR. This better characterisation of the ice cloud radiative properties should allow to improve the understanding of their role in the Earth radiation budget and in climate.

Acknowledgements. The deployment of REFIR-PAD in Antarctica was supported by the Italian National Program for Research in Antarctica PNRA (Programma Nazionale di Ricerche in Antartide) under the following projects: 2009/A04.03, 2013/AC3.01, and 2013/AC3.06. The authors are gratefully to the research group of the Institute of Applied Physics (CNR-Florence) composed by Bruno Carli, Simone Ceccherini, Marco Gai, Samuele Del Bianco, Ugo Cortesi, Marco Ridolfi, Piera Raspollini, Flavio Barbara, for the precious and fruitful discussions.

Atmos. Meas. Tech. Discuss., doi:10.5194/amt-2016-181, 2016
Manuscript under review for journal Atmos. Meas. Tech.
Published: 12 August 2016

Atmospheric Measurement Techniques Discussions

References

Baran A. J., The dependence of cirrus infrared radiative properties on ice crystal geometry and shape of the size-distribution function, Q. J. R. Meteorol. Soc. (2005), 131, pp. 1129–1142.

Baran A. J., The impact of cirrus microphysical and macrophysical properties on upwelling far infrared spectra, Q. J. R. Meteorol. Soc., 133, 1425–1437 ,2007.

Baran A. J., A review of the light scattering properties of cirrus, Journal of Quantitative Spectroscopy and Radiative Transfer, Volume 110, 1239–1260, 2009.

Bianchini G., Palchetti L., Carli B., A wide-band nadir-sounding spectroradiometer for the characterization of the Earth's outgoing long-wave radiation, Proc. SPIE, 6361, 2006.

Bianchini G., Carli B.,Cortesi U.,Del Bianco S.,Gai M.,Palchetti L., Test of far-infrared atmospheric spectroscopy using wide-band balloon-borne mmeasurements of the upwelling radiance,Journal of Quantitative Spectroscopy & Radiative Transfer 109 (2008) 1030–1042.

Birch K. P. and Downs M. J., Correction to the Updated Edlén Equation for the Refractive Index of Air, Metrologia, Vol.31, No. 315, 1994.

Broyden C.G., A class of methods for solving nonlinear simultaneous equations, Mathematics of computation, 19, 577-593, 1965

Ceccherini S. and Ridolfi M., Technical Note: Variance-covariance matrix and averaging kernels for the Levenberg-Marquardt solution of the retrieval of atmospheric vertical profiles, Atmospheric Chemistry and Physics, 10, 3131-3139, 2010.

Clough S. A.,Shephard M. W.,Mlawer E. J., Delamere J. S.,Iacono M. J.,Cady-Pereira K.,Boukabara S.,and Brown P. D., Atmospheric radiative transfer modeling: a summary of the AER codes, Short Communication, J. Quant. Spectrosc. Radiat. Transfer, 91, 233-244, 2005.

Deeter M. N. and Evans K. F., A hybrid Eddington-single scattering radiative transfer model for computing radiances from thermally emitting atmospheres, J. Quant. Spectrosc.Radiat. Transfer 60, 4,635–648, 1998.

De Leon R. R. and Haigh D. J.,Infrared properties of cirrus clouds in climate models, Q. J. R. Meteorol. Soc. 133: 273–282 (2007).

Del Guasta M.,Morandi M. and Stefanutti L., One year of cloud lidar data from Dumont D'Urville (Antarctica) 1. General overview of geometrical and optical properties, Journal of Geophysical Research, Volume 98, No. D10, 18575-18587, 1993.

Fisher R. A., The logic of inductive inference, J.R. Stat. Soc. 98(1), 39–54 (1935).

Fu. Q., Parameterization of radiative processes in vertically nonhomogeneous multiple scattering atmospheres. PhD. dissertation, University of Utah, 259 pp. [Avalaible from University Microfilm, 305 N. Zeeb Rd, Ann Arbor,MI 48106]

Fu Q. and Liou K. N. , Parameterization of the radiative properties of cirrus clouds, J. Atmos. Sci., 50, 2008-2025, 1993.

Fu Q., An accurate parameterization of the solar radiative properties of cirrus clouds for climate models, Journal of Climate, Volume 9, 2058-2082, 1996.

Fu Q. ,Yang P., Sun W.B. , An accurate parameterization of the infrared radiative properties of cirrus clouds for climate models, American Meteorological Society, Volume 11, Issue 9, 2223-2237,1998.

Gavin H.P., The Levenberg-Marquardt method for nonlinear least squares curve-fitting problems, Department of Civil and Environmental Engineering, Duke University, (September 2015)

Harries J.,Carli B. ,Rizzi R.,Serio C.,Mlynczak M.,Palchetti, L.,Maestri T.,Brindley H., and Masiello G., The Far Infrared Earth, Reviews of Geophysics, 46, RG4004, 2008.

Heymsfield A. J.,Matrosov S.,Baum B., Ice water path-optical depth realationship for cirrus and deep stratiform ice cloud layers, American Meteorological Society, 1369–1390, 2003.

Joseph J. H. and Wiscombe W. J., The delta-Eddington approximation for radiative flux transfer, Journal of the Atmospheric Sciences, 33, 2452–2459, 1976.

Kiehl J. T. and Trenberth K. E., Earth's annual global mean energy budget, Bulletin of the American Meteorological Society, Vol. 78, No. 2, 197-207, 1997.

Linch D., K. Sassen, D. O. Star and Sthephens G., Cirrus, Book, Oxford University Press, Inc., 2002.

Liou, K., Influence of cirrus clouds on weather and climate processes:a global perspective, Monthly Weather Review, Volume 114, 1167-1199,1986.

Liou K. N.,Gu Y.,Yue Q., and McFarguhar G., On the correlation between ice water content and ice crystal size and its application to radiative transfer and general circulation models, Geophysical Research Letters, Vol. 35, L13805, doi:10.1029/2008GL033918, 2008.

Maestri T.,Rizzi R. ,Tosi E.,Veglio P.,Palchetti L.,Bianchini G.,Di Girolamo P.,Masiello G.,Serio C. ,Summa D., Analysis of cirrus cloud spectral signatures in the far infrared, J. Quant. Spectrosc. Radiat. Transfer, 141, 49–64, 2014.

Marquardt D. W., An algorithm for least-squares estimation of non-linear parameters, SIAM J. Appl. Math., 11, 431-441, 1963.

Nelder J. A. and Mead R., A Simplex Method for Function Minimization, The Computer Journal, Volume 7 Issue 4, 308-313. doi: 10.1093/comjnl/7.4.308, 1965.

Klett J. D., Stable analytical inversion solution for processing lidar returns, Applied Optics, Vol.20,No.2, 1981.

Palchetti L. and Lastrucci D., Spectral noise due to sampling errors in Fourier-transform spectroscopy, Applied Optics, Vol. 40, No. 19, 2001.

Palchetti L.,Bianchini G.,Castagnoli F.,Carli B.,Serio C.,Esposito F.,Cuomo V.,Rizzi R.,Maestri T., Breadboard of the Fourier transform spectrometer for the Radiation Explorer in the Far Infrared (REFIR) atmospheric mission, Applied Optics, Vol.44, No.14, pp.2870-2878, 2005.

Palchetti L.,Bianchini G.,Carli B.,Cortesi U., and Del Bianco S., Measurement of the water vapour vertical profile and of the Earth's outgoing far infrared flux, Atmos. Chem. Phys., 8, 2885–2894, 2008.

Palchetti L.,Bianchini G.,Di Natale G.,Del Guasta M., Far-Infrared radiative properties of water vapor and clouds in Antarctica, Bulletin of American Meteorological Society, http://dx.doi.org/10.1175/BAMS-D-13-00286.1 G. ,Volume 96, Issue 9, 2015.

Palchetti L.,Di Natale G., and Bianchini G., Remote sensing of cirrus microphysical properties using spectral measurements over the full range of their thermal emission, Journal of Geophysical Research, 2016.

Rathke C. and Fisher J., Retrieval of cloud microphysical properties from thermal infrared observations by a fast iterative radiance fitting method, Journal of atmospheric and oceanic technology, Volume 17, 1509-1524, 2000.

Remedios J. J., Leigh R. J., Waterfall A. M., Moore D. P., Sembhi H., Parkes I., Greenhough J., Chipperfield M.P., and Hauglustaine D.: MIPAS reference atmospheres and comparisons to V4.61/V4.62 MIPAS level 2 geophysical data sets, Atmos. Chem. Phys. Discuss., 7, 9973-10017, doi:10.5194/acpd-7-9973-2007, 2007.

Rodgers, C. D.: Inverse Methods for Atmospheric Sounding: Theory and Practice, World Scientific Pub Co Inc, 2000. 5559, 5580, 5581, 5589

Turner D.D., Arctic Mixed-Phase Cloud Properties from AERI Lidar Observations: Algorithm and Results from SHEBA, Journalof Applied Meteorology, Vol. 44, 427-444, 2005.

Turner D.D.,Ackerman S.A.,Baum B.A.,Revercomb H.E.,Yang P., Cloud Phase Determination Using Ground-Based AERI Observations at SHEBA, Journal of Applied Meteorology, Vol. 42, 710−715, 2003.

Vömel H.,Selkirk H.,Miloshevich L,Valverde-Canossa J.,Valdès J.,Kyrö E.,Kivi R.,Stolz W.,Peng G., and Diaz J. A., Radiation Dry Bias of the Vaisala RS92 Humidity Sensor, Journal of atmospheric and oceanic technology, Volume 24, 953-963, 2007.

Atmos. Meas. Tech. Discuss., doi:10.5194/amt-2016-181, 2016
Manuscript under review for journal Atmos. Meas. Tech.
Published: 12 August 2016

Yang P.,Gao B. C.,Baum B. A.,Hu Y. X. ,Wiscombe W. J.,Tsay S. C., Winker D. M., and Nasiri S. L., Radiative properties of cirrus clouds in the infrared (8 – 13 mm) spectral region, J. Quant. Spectrosc. Radiat.Transfer, 70, 473 – 504, 2001.

Yang P., Wei H.,Huang H.-L. ,Baum B. A.,Hu Y. X.,Kattawar G. W.,Mishchenko M. I., and Fu Q. , Scattering and absorption property database for nonspherical ice particles in the near-through far-infrared spectral region, Applied Optics, 44, 26 (2005).

Wild M.,Folini D.,C. Schär C.,Loeb N.,Dutton E. G.,König-Langlo G., The global energy balance from a surface perspective, Clim Dyn (2013) 40:3107–3134 DOI 10.1007/s00382-012-1569-8

Wiser K. and Yang P., Average ice crystal size and bulk short-wave single-scattering properties of cirrus clouds, Atmospheric Research 49 (1998) 315–335.

Atmos. Meas. Tech. Discuss., doi:10.5194/amt-2016-181, 2016
Manuscript under review for journal Atmos. Meas. Tech.
Published: 12 August 2016

Atmospheric Measurement Techniques Discussions

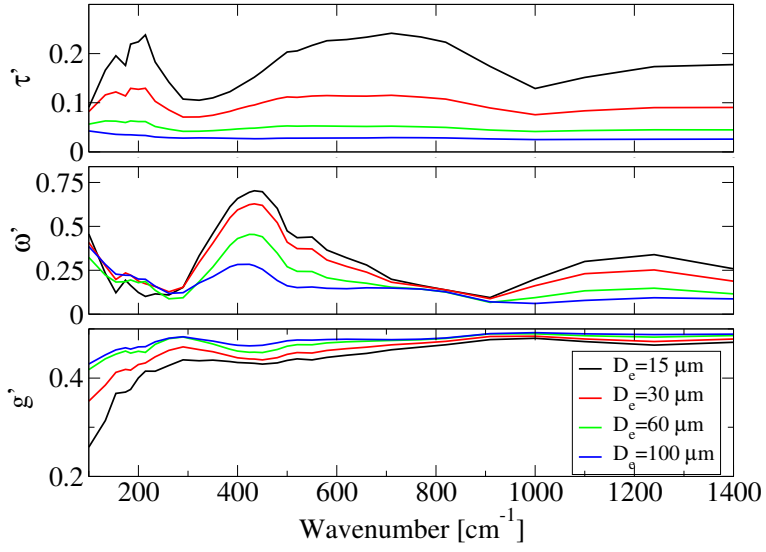

Figure 1. Scaled optical parameters for different values of D_{ge}, 15,30, 60 and 100 μm respectively. The optical depth τ is calculated for IWP=2 gm^{-2}.

Atmos. Meas. Tech. Discuss., doi:10.5194/amt-2016-181, 2016
Manuscript under review for journal Atmos. Meas. Tech.
Published: 12 August 2016

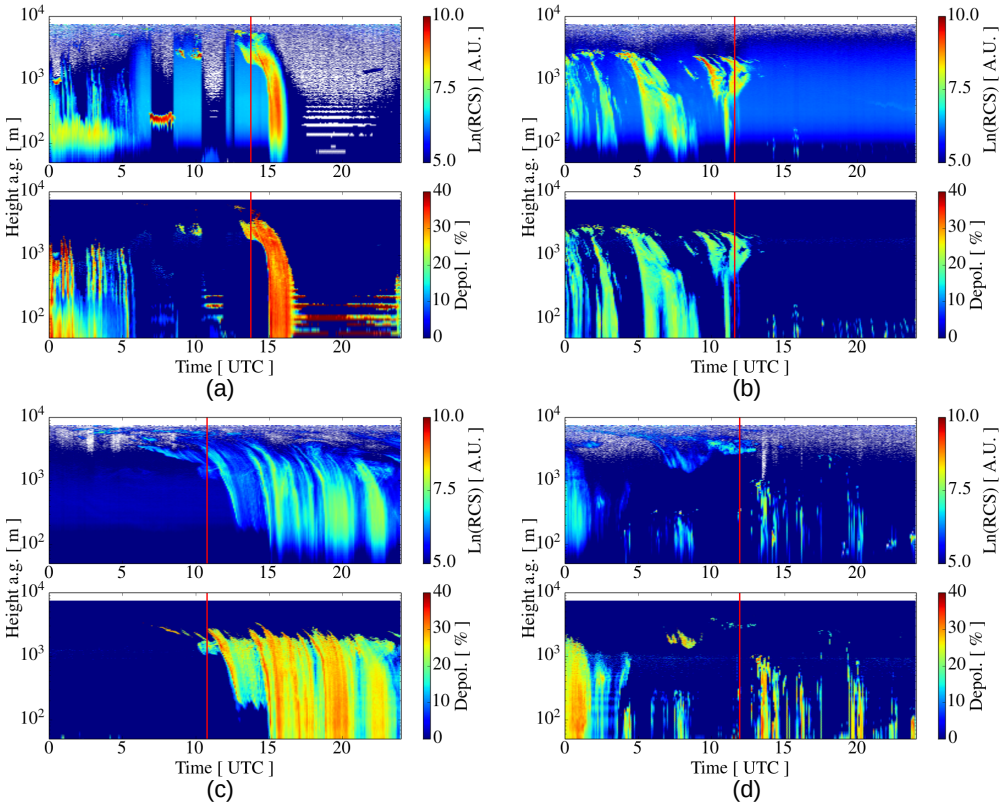

Figure 2. Colour maps of RCS and depolarisation signals performed by the lidar at Dome-C for different days and seasons. The panels show the passage of an ice cloud in Summer on 12 February 2014 (a), in Autumn on 2 April 2014 (b), in Winter on 10 August 2014 (c), and in Spring on 1 October 2014 (d). The red lines indicate the times at which the analysed spectra were acquired.

Atmos. Meas. Tech. Discuss., doi:10.5194/amt-2016-181, 2016
Manuscript under review for journal Atmos. Meas. Tech.
Published: 12 August 2016

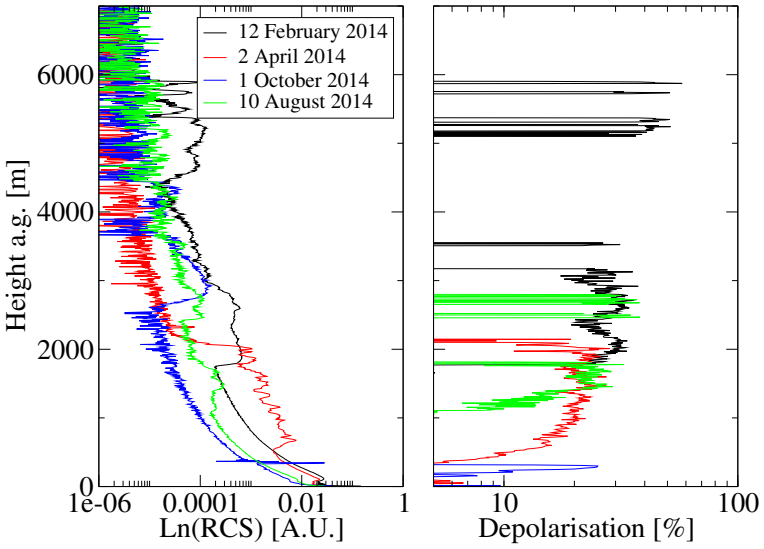

Figure 3. Logarithmic RCS and depolarisation signal corresponding to the four selected days. The first one is in arbitrary unit as a function of the height in km above ground and depolarisation.

Atmos. Meas. Tech. Discuss., doi:10.5194/amt-2016-181, 2016
Manuscript under review for journal Atmos. Meas. Tech.
Published: 12 August 2016

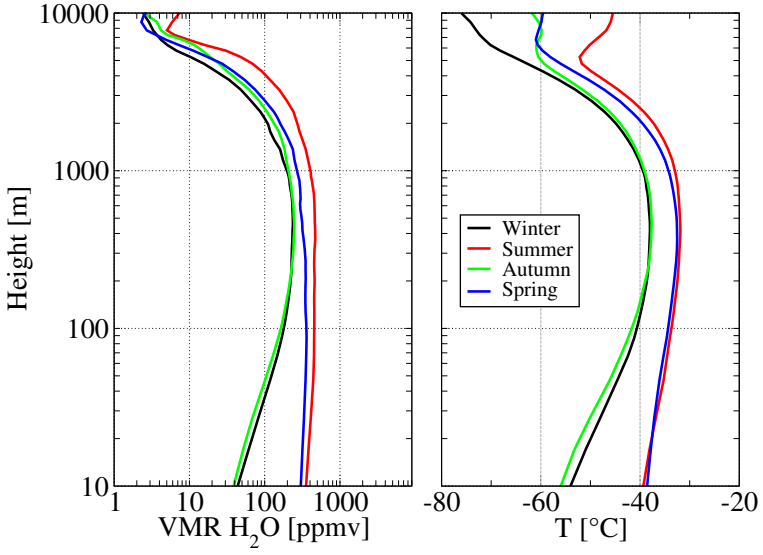

Figure 4. Plotting of the four seasonal climatological profiles of water vapour VMR (left panel) and temperature (right panel) used as initial guesses in the fitting procedure.

Atmos. Meas. Tech. Discuss., doi:10.5194/amt-2016-181, 2016
Manuscript under review for journal Atmos. Meas. Tech.
Published: 12 August 2016

Atmospheric Measurement Techniques Discussions

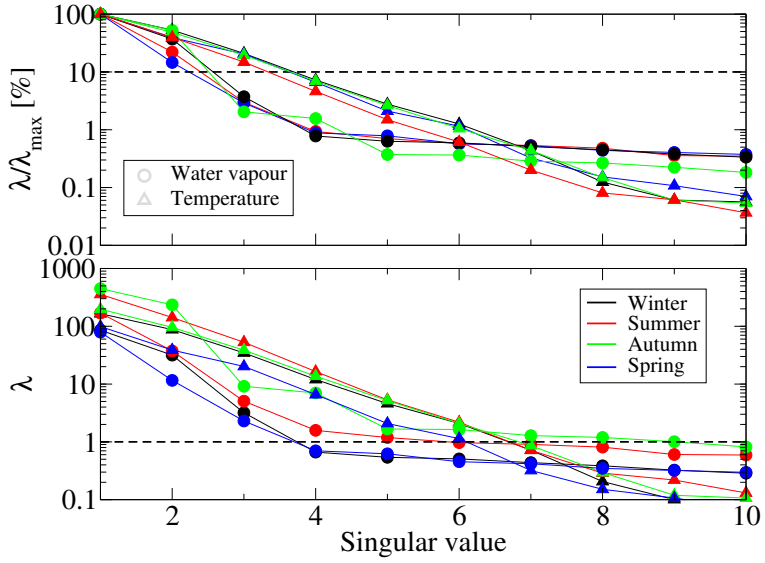

Figure 5. In the upper panel the trend of the ratios between the the singular values and the maximum for water vapour (circles) as well as the temperature (triangles) are reported in percentage for every season (different colours). Furthermore the threshold of the singular independent states represented by the black-dashed line, identifies the limit value above which the states are neglected. In the lower panel the absolute values of the singular values are also shown and the black-dashed line is the threshold below which the values corresponding to the states contribute only as the noise.

Atmos. Meas. Tech. Discuss., doi:10.5194/amt-2016-181, 2016
Manuscript under review for journal Atmos. Meas. Tech.
Published: 12 August 2016

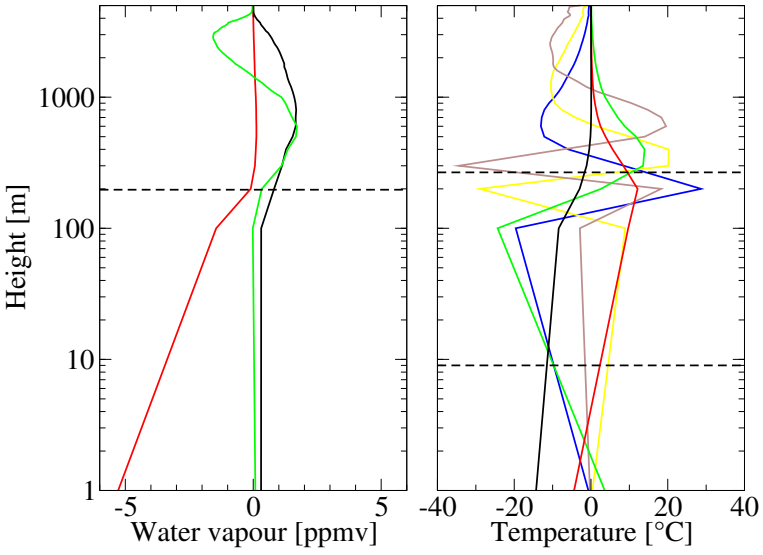

Figure 6. First back-transformed singular vectors of $\widetilde{\mathbf{K}}$ of water vapour and temperature for the singular values greater than about unity calculated by using the winter climatology.

Atmos. Meas. Tech. Discuss., doi:10.5194/amt-2016-181, 2016
Manuscript under review for journal Atmos. Meas. Tech.
Published: 12 August 2016

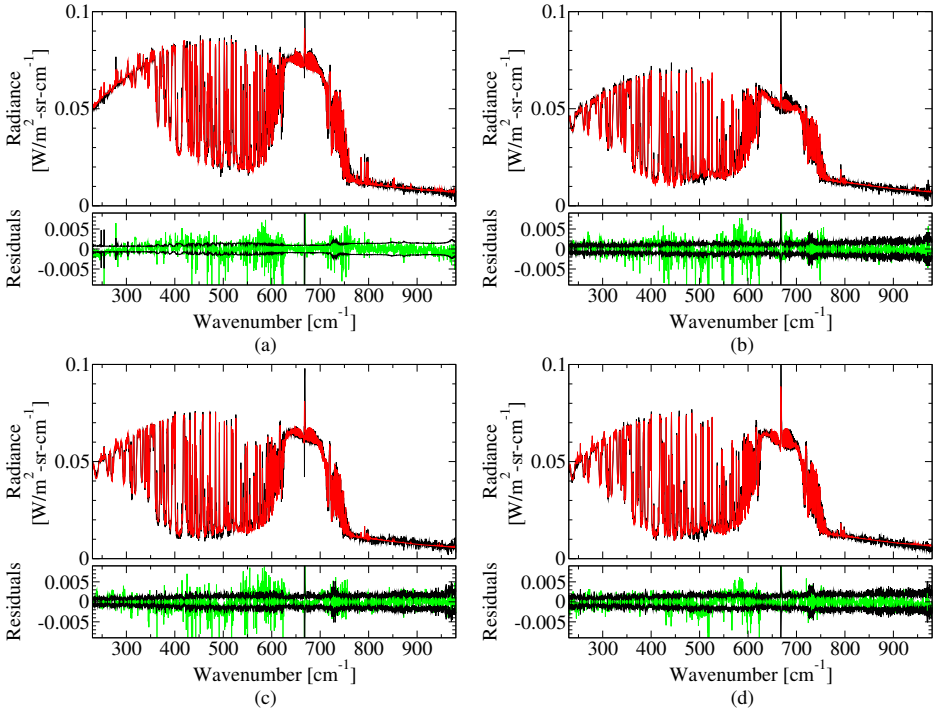

Figure 7. Results of fitting. The comparisons of the synthetic spectra (red) provided by the retrieval with the measurements (black) are shown. The days are the same as in Fig. 2. The lower panels show the comparisons of the residuals (green) with the measurement uncertainty.

Atmos. Meas. Tech. Discuss., doi:10.5194/amt-2016-181, 2016
Manuscript under review for journal Atmos. Meas. Tech.
Published: 12 August 2016

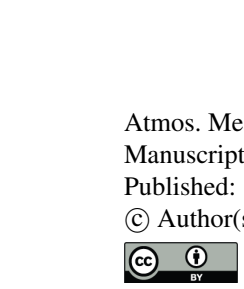

Atmospheric Measurement Techniques Discussions

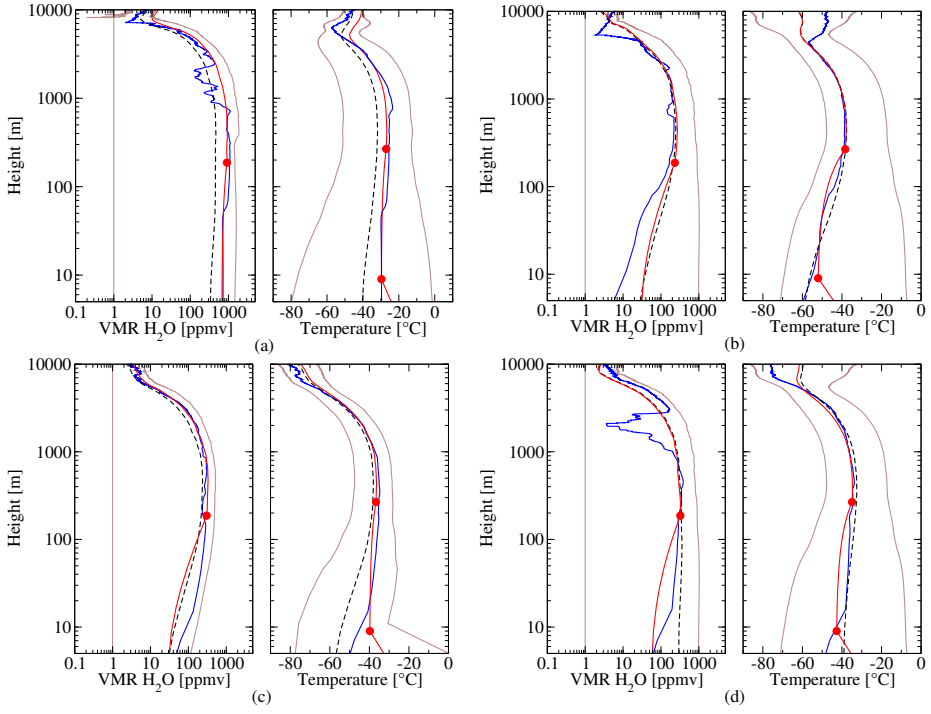

Figure 8. Retrieved profiles of water vapour VMR and temperature (red) for the selected days of Fig. 7. This figures show the comparison with radiosounding profiles in blue colour and the initial guess (dashed black line). The brown lines indicates the physical limits, set to be 3-σ of the climatology, used to constrain the retrieval.

Atmos. Meas. Tech. Discuss., doi:10.5194/amt-2016-181, 2016
Manuscript under review for journal Atmos. Meas. Tech.
Published: 12 August 2016

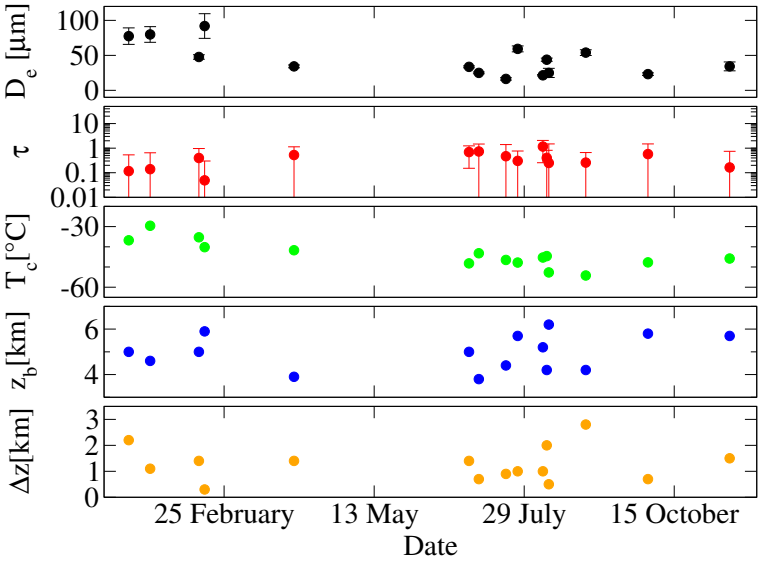

Figure 9. Time evolution of the clouds parameters. Starting from the upper panel the generalised effective diameter, optical depth, cloud temperature, bottom height z_b and thickness Δz are shown.

Atmos. Meas. Tech. Discuss., doi:10.5194/amt-2016-181, 2016
Manuscript under review for journal Atmos. Meas. Tech.
Published: 12 August 2016

Atmospheric Measurement Techniques Discussions

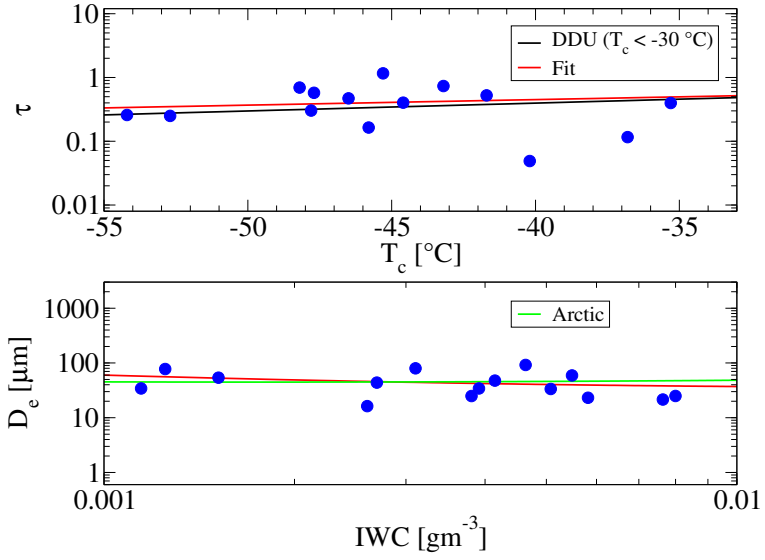

Figure 10. Retrieved data (blue dots) and fit (red line) of optical depth as a function of temperature are compared with the Dumont D'Urville (DDU) statistics (black line) in the upper panel and with the Arctic D_e – IWC distribution (Liou, 2008) (green line) in the lower panel.